Rotating ³He droplets

Martí Pi (iD) , Francesco Ancilotto, and Manuel Barranco (iD)

View Online   Export Citation   CrossMark

Rotating ³He droplets

Martí Pi,[1,2,a] (iD) **Francesco Ancilotto,**[3,4,b] **and Manuel Barranco**[1,2,5,c] (iD)

AFFILIATIONS

[1] Departament FQA, Facultat de Física, Universitat de Barcelona, Diagonal 645, 08028 Barcelona, Spain

[2] Institute of Nanoscience and Nanotechnology (IN2UB), Universitat de Barcelona, Barcelona, Spain

[3] Dipartimento di Fisica e Astronomia "Galileo Galilei" and CNISM, Università di Padova, via Marzolo 8, 35122 Padova, Italy

[4] CNR-IOM Democritos, via Bonomea, 265 - 34136 Trieste, Italy

[5] Université Toulouse 3, Laboratoire des Collisions, Agrégats et Réactivité, IRSAMC, 118 route de Narbonne, F-31062 Toulouse Cedex 09, France

[a] Author to whom correspondence should be addressed: marti@fqa.ub.edu
[b] Electronic mail: francesco.ancilotto@pd.infn.it
[c] Electronic mail: manuel@fqa.ub.edu

ABSTRACT

Motivated by recent experiments, we study normal-phase rotating ³He droplets within density functional theory in a semi-classical approach. The sequence of rotating droplet shapes as a function of angular momentum is found to agree with that of rotating classical droplets, evolving from axisymmetric oblate to triaxial prolate to two-lobed shapes as the angular momentum of the droplet increases. Our results, which are obtained for droplets of nanoscopic size, are rescaled to the mesoscopic size characterizing ongoing experimental measurements, allowing for a direct comparison of shapes. The stability curve in the angular velocity–angular momentum plane shows small deviations from the classical rotating drop model predictions, whose magnitude increases with angular momentum. We attribute these deviations to effects not included in the simplified classical model description of a rotating fluid held together by surface tension, i.e., to surface diffuseness, curvature, and finite compressibility, and to quantum effects associated with deformation of the ³He Fermi surface. The influence of all these effects is expected to diminish as the droplet size increases, making the classical rotating droplet model a quite accurate representation of ³He rotation.

Published under license by AIP Publishing. https://doi.org/10.1063/5.0007959

I. INTRODUCTION

Helium is the only element in nature that may condense into macroscopic liquid samples at temperatures close to absolute zero. These systems can be made of either pure isotope or of ³He–⁴He isotopic mixtures. Below a temperature (T) that depends on the isotope (2.17 K for ⁴He, 2.7 mK for ³He) and also on the isotopic composition in the case of mixtures,[1] these remarkable fluids undergo a well-known normal-to-superfluid phase transition. These properties, which are a manifestation at the microscale of the quantum nature of low temperature liquid helium, have drawn relentless scientific attention since they were uncovered about 80 years ago. A first hand, personal view of the first stages in the development of helium atom beams and droplets has been given by Toennies.[2]

In more recent years, helium droplets have been the subject of renewed interest, both experimentally and theoretically. In the experiments, ⁴He droplets are produced at $T \sim 0.37$ K;[3] hence, they are superfluid and represent ideal ultra-cold matrices for spectroscopy studies of captured molecular impurities[4] and for addressing superfluidity at the nanoscale.[5] At variance, ³He droplets are created at $T \sim 0.15$ K;[6] hence, they are in the normal phase. For this reason, they are expected to behave more as classical viscous fluid droplets. ³He droplets have been the subject of far less studies than ⁴He droplets. The activity on ³He droplets has partially been reviewed in Refs. 7 and 8.

Recently, large ⁴He droplets made of 10^8–10^{11} atoms have been created by the hydrodynamic instability of a liquid helium jet passing through the nozzle of the molecular beam apparatus, as reviewed in Ref. 9. Helium drops, which are produced in the normal,

non-superfluid phase, may acquire angular momentum during the passage of the fluid through the nozzle before cooling down and become superfluid. Such droplets could be analyzed one-by-one by x-ray and extreme ultraviolet (XUV) light and intense high harmonics sources,[10,11] which have allowed to determine their shapes and, doping them with Xe atoms,[10,12] the presence of vortices, thus stressing their superfluid nature.

One of the intriguing findings of Refs. 10 and 11 was that the sequence of shapes of the spinning superfluid ^{4}He droplets is in accordance with that of classical rotating droplets.[13–16] It has been shown that it is the presence of quantized vortices that confers to the superfluid droplets the appearance of classical viscous droplets when they are set in rotation.[17]

It is quite natural to ask whether droplets made of liquid ^{3}He do indeed rotate as classical droplets made of normal fluid, and whether their properties may be described by a more microscopic approach instead of that successfully used for viscous liquid droplets.[13–16] Besides, a proper microscopic description of pristine ^{3}He droplets is a necessary step toward the study of mixed ^{3}He–^{4}He droplets, which represents the prototype of strongly correlated Bose–Fermi liquid mixtures. These are the goals of the present paper.

In this work, we describe deformed droplets within Density Functional Theory (DFT) formalism for liquid ^{3}He.[18] At the experimental temperatures, thermal effects on the energetics and morphology of the droplet are negligible,[19] so we shall use a $T = 0$ method. Zero temperature means here a very low temperature, but above the ∼2.7 mK, at which ^{3}He becomes superfluid.

As ^{3}He atoms are fermions, the DFT–Kohn–Sham (DFT–KS) approach should be the method of choice for this study. It has been used in the past to address spherical ^{3}He droplets made of up to a few hundred atoms.[20] Deformed (doped) ^{3}He droplets with a few tens of ^{3}He atoms have been addressed as well within such an approach.[19] Let us mention that diffusion Monte Carlo calculations have been made for pure ^{3}He$_N$ droplets up to $N = 34$,[21] and exact diagonalization results exist for ^{3}He$_4$ clusters doped with Cl$_2$.[22]

Unfortunately, the DFT–KS approach is unfeasible for large, deformed ^{3}He droplets as the ones investigated here. The use of a DFT–KS scheme is unavoidable when shell effects are expected to play a role as in small droplets;[7,19] however, for the experimental droplet sizes, of the order of 10^8–10^{10} atoms,[23] the shell structure cannot play any substantial role. Besides, temperatures of the order of 100 mK have been found to wash out the shell structure of mixed ^{3}He–^{4}He droplets.[24] Under these conditions, the use of a semiclassical approximation to the DFT formalism, as the one described in the following, is fully justified. The finite viscosity of ^{3}He at the experimental temperatures adds further justification to using classical or semiclassical methods to address the rotating ^{3}He droplets.

We have thus resorted to a semiclassical approach, treating the ^{3}He droplets in the DFT plus rotating Thomas–Fermi (TF) framework, which has successfully been used in nuclear physics to address deformed nuclei.[25–27] The DFT-TF method is the only realistic framework that has the virtue of making numerical simulations affordable and that can be extended in a natural way to mixed helium droplets at the experimental conditions.[7]

This work is organized as follows. In Sec. II, we present the DFT-TF method used to describe the ^{3}He droplets. The results are discussed in Sec. III, and a summary and outlook are given in Sec. IV. Details on the rotating TF approximation are given in the Appendix.

II. MODEL

Within DFT, the total energy E of a ^{3}He$_N$ droplet at zero temperature is written as a functional $\mathcal{E}_c$ of the ^{3}He atom density ρ, here taken from Ref. 28,

$$E[\rho] = \int d\mathbf{r} \frac{\hbar^2}{2m^*} \tau + \int d\mathbf{r}\, \mathcal{E}_c[\rho]. \tag{1}$$

The first term is the kinetic energy of ^{3}He with an effective mass m^*, and τ is the kinetic energy density, both depending on ρ. In the TF approximation of Ref. 28 (see also Ref. 18),

$$\tau = \frac{3}{5}(3\pi^2)^{2/3}\rho^{5/3} + \frac{1}{18}\frac{(\nabla\rho)^2}{\rho}. \tag{2}$$

The second term in the above equation is a Weizsäcker-type gradient correction that is necessary in order to have helium densities with an exponential fall-off at the surface.[29] The energy functional Eq. (1) together with the TF approximation Eq. (2) has been found to accurately reproduce the equation of state of the homogeneous system and the correct value for the ^{3}He surface tension.[28]

In this work, the number of ^{3}He atoms is fixed to $N = 1500$. The droplet equilibrium configuration is obtained by solving the Euler–Lagrange (EL) equation arising from functional variation of Eq. (1),

$$\frac{\delta}{\delta\rho}\left\{\frac{\hbar^2}{2m^*}\tau + \mathcal{E}_c\right\} = \mu, \tag{3}$$

where μ is the ^{3}He chemical potential. Defining $\Psi = \sqrt{\rho}$, Eq. (3) can be written as a Schrödinger-like equation,[28]

$$\mathcal{H}[\rho]\,\Psi = \mu\Psi, \tag{4}$$

where $\mathcal{H}$ is the one-body effective Hamiltonian that results from the functional variation.

When the rotating droplet—made of fermions in the normal phase—is addressed in the TF approximation, the Fermi sphere is shifted by the motion of the droplet as a whole; this adds to the droplet total energy a rotational term that has the rigid body appearance,[25]

$$E[\rho] \to \mathcal{R}[\rho] = E[\rho] + \frac{1}{2}\mathcal{I}\omega^2, \tag{5}$$

where $\mathcal{R}[\rho]$ is the Routhian of the system and $\mathcal{I}$ is defined in Eq. (7). Details are given in the Appendix.

To deposit angular momentum in a droplet rotating with angular velocity ω about a given axis (the z-axis here), it is convenient to work in the fixed-droplet frame of reference (corotating frame at angular velocity ω), i.e., we consider

$$E'[\rho] = \mathcal{R}[\rho] - \hbar\omega\langle L\rangle = E[\rho] - \frac{1}{2}\mathcal{I}\omega^2, \tag{6}$$

where $\hbar\langle L\rangle = \mathcal{I}\omega$ is the ^{3}He angular momentum obtained from the classical rigid body moment of inertia $\mathcal{I}$,

$$\mathcal{I} = m \int d\mathbf{r}\,(x^2 + y^2)\rho(\mathbf{r}). \qquad (7)$$

We want to stress that the rigid body moment of inertia is not an imposed ingredient to the DFT-TF framework. It arises naturally from the TF approximation, as shown in the Appendix. In the more general DFT–KS framework, the rigid body moment of inertia similarly appears within the so-called "cranking model," as thoroughly discussed for nucleons rotating in the mean field created by the atomic nucleus.[30–32]

In the corotating frame, we have to look for solutions of the EL equation resulting from the functional variation of $E'[\rho]$,

$$\left\{\mathcal{H}[\rho] - \frac{m}{2}\,\omega^2(x^2 + y^2)\right\}\Psi(\mathbf{r}) = \mu\,\Psi(\mathbf{r}). \qquad (8)$$

The results presented in this work have been obtained adapting the 4He-DFT BCN-TLS computing package[33] to the case of ^{3}He atoms in the TF approximation. Details on how Eqs. (3) and (8) are solved can be found in Refs. 8 and 34 and references therein. In short, we work in Cartesian coordinates, make extensive use of the fast Fourier transform to compute the convolutions entering the definition of the effective Hamiltonian $\mathcal{H}$, and obtain the droplet equilibrium configuration by imaginary-time relaxation. To determine the prolate branch, we have iterated on ω to get the desired L_z value.[13–15,17]

The experimental droplets have a radius in the 100–200 nm range.[23] A comparison between the calculated nanoscopic DFT droplets and the experimental ones thus requires some scaling procedure. To this end, we have introduced a dimensionless angular momentum Λ and angular velocity Ω, as done for classical drops,[13–15]

$$\Omega \equiv \sqrt{\frac{m\rho_0 R^3}{8\gamma}}\,\omega = \left[\frac{2m}{\hbar^2}\frac{3}{64\pi\gamma}N\right]^{1/2}\hbar\omega,$$

$$\Lambda \equiv \frac{\hbar}{\sqrt{8\gamma R^7 m\rho_0}}\,L_z = \left[\frac{\pi}{3\gamma r_0^4}\frac{\hbar^2}{2m}\right]^{1/2}\frac{L_z}{N^{7/6}}. \qquad (9)$$

In the above expressions, γ and ρ_0 are the surface tension and liquid atom density at zero temperature and pressure, R is the sharp radius of the spherical droplet when $L_z = 0$, and r_0 is the bulk radius defined such that $4\pi r_0^3\rho_0/3 = 1$; hence, $R = r_0 N^{1/3}$. For liquid ^{3}He, these values are $\gamma = 0.113$ K Å^{-2} and $\rho_0 = 0.0163$ Å^{-3} ($r_0 = 2.45$ Å). Besides, $\hbar^2/m = 16.08$ K Å^2. Liquid helium is fairly incompressible, and hence, the volume of the deformed configurations is also taken as $V = 4\pi R^3/3$.

In classical model approaches,[13–15] it is assumed that the equilibrium configuration of the rotating droplet is solely determined by the balance between the rotational and surface energies. This makes the problem amenable to a dimensionless formulation, where the Routhian can be expressed in terms of the Λ and Ω variables that characterize the equilibrium configuration irrespective of the droplet size, and consequently, the results are universal. This is quite not so in microscopic approaches such as DFT, for instance, where the droplets have a large but finite incompressibility and

also a surface finite width instead of a sharp interface separating the fluid from the vacuum, as assumed in classical models. In general, not only surface and rotational energies matter to determine the shape of the droplet at equilibrium; volume and quantum kinetic energy terms do change with deformation, and this must be taken into account as the present DFT approach does. Curvature energy, naturally incorporated in the DFT approach, contributes as well to the energy of the droplet, and its effect increases with the droplet deformation, thus likely affecting the location of the higher angular momentum equilibrium configurations in the Λ-Ω plane.

Consequently, some differences are expected to show up when comparing the results obtained in classical and DFT approaches, especially for small drops for which the surface thickness is not negligible compared to their radius. This is shown in Fig. 1 for the ^{3}He$_{1500}$ and ^{4}He$_{1500}$ droplets as well. The ^{3}He surface is thicker as a natural consequence of the quantum zero point motion, which is larger for ^{3}He than that of ^{4}He because its mass is smaller. Experiments on the free surface of liquid ^{4}He films adsorbed on a solid substrate at $T = 0.45$ K have yielded surface widths between 5.3 ± 0.5 Å (thin films) and 6.5 ± 0.5 Å (thick films).[35]

For any stationary configuration obtained by solving Eq. (8), a sharp density surface is determined by calculating the locus at which the helium density equals $\rho_0/2$; for a spherical distribution, this corresponds to a sphere of radius $R = r_0 N^{1/3}$. In the case of deformed droplets, three lengths are introduced corresponding to the distances from the center of mass (COM) of the droplet to the sharp surface along the rotation axis (c_z), the largest distance from the COM to the sharp surface along an axis perpendicular to the rotation axis (a_x), and the distance of the COM to the sharp surface in the direction perpendicular to the other two (b_y). One expects,[36] and our calculations confirm, that $a_x \geq b_y > c_z$. These lengths have been used to define two ratios: a_x/c_z and a_x/b_y; the latter one will be referred to as "aspect ratio" (AR); these ratios facilitate the comparison between different models and with the experimental results as well.
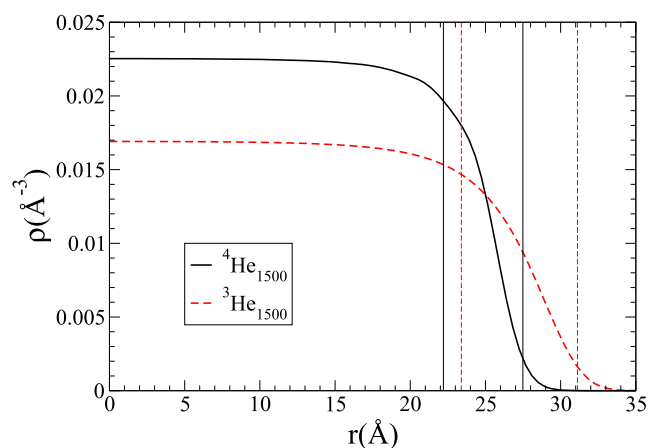

FIG. 1. Density profile of the ^{3}He$_{1500}$ and ^{4}He$_{1500}$ spherical droplets. The region between the thin vertical lines is the surface region defined as that where the helium density falls from $0.9 \times \rho_0$ to $0.1 \times \rho_0$.

III. RESULTS AND DISCUSSION

Table I collects the relevant features of the calculated stationary configurations. We have found that the droplet fissions for a value of Λ between 2.05 and 2.1.

Figure 2 shows three characteristic prolate ^{3}He$_{1500}$ droplets whose shapes evolve from ellipsoidal to capsule-like to two-lobed as angular momentum increases. It is worth mentioning that vortex-free ^{4}He droplet configurations are more stretched than the ^{3}He ones for the same Λ value. In particular, the Λ = 1.5 ^{4}He configuration is already two-lobed and has a_x/c_z = 3.578 (see the supplementary material of Ref. 17). This is due to the superfluid character of the ^{4}He droplets. In the absence of vortex arrays, only capillary waves can carry angular momentum, and for a given Λ, this requires larger deformations than in the ^{3}He case. This can be seen easily in the case of vortex-free, strictly ellipsoidal droplets, where the angular momentum is proportional to $(a_x^2 - b_y^2)^2$ (see, e.g., Ref. 37).

Blood-cell shapes (i.e., oblate droplets thinner in the center and thicker at the periphery) have been observed for spheroidal ^{4}He droplets beyond the classical stability limit.[10] Metastable oblate ^{3}He droplets display a minute depletion at their center, as shown in Fig. 3, for the largest angular velocity considered in our calculations, Ω = 0.6364.

To determine the oblate-to-prolate bifurcation point, one has to compare the Routhian $\mathcal{R}[\rho]$—defined in Eq. (5)—of the oblate and prolate configurations for the same Λ value; the configuration with the smaller $\mathcal{R}$ is the equilibrium one.[13] Within the classical model approach to droplets subject only to surface tension and centrifugal forces, the bifurcation point is $(\Omega_{cl}, \Lambda_{cl})$ = (0.55, 1.20).[13,14,16] Within the DFT-TF approach to ^{3}He droplets, the bifurcation point is at $(\Omega, \Lambda) \sim$ (0.57, 1.28), as shown in Fig. 4.

Figure 5 shows the rescaled angular velocity Ω vs rescaled angular momentum Λ. For a fixed Ω, the DFT result is shifted to the right of the classical one. The existence of a surface width is expected to produce some shift. Indeed, due to the density spill-out beyond the sharp density surface, the droplets described realistically have more fluid away from the rotation axis than if the surface is sharp as in classical models. Hence, for a given Ω, DFT configurations must have a larger moment of inertia and thus a larger Λ value.[38]

Figure 5 also shows the $\Omega(\Lambda)$ relationship for vortex-free ^{4}He droplets—where angular momentum is associated with giant capillary waves—obtained in Ref. 17. It is worth seeing the completely different behavior between a rotational (^{3}He) and an irrotational—potential—fluid (superfluid ^{4}He).

Figure 6 shows the aspect ratio AR as a function of Λ extracted from the information in Table I. For comparison, the classical result is also shown.[15] Figure 7 shows the a_x/c_z ratio as a function of Λ.

We recall that the x-ray diffraction images that are observed in experiments on spinning ^{4}He and ^{3}He droplets as well do not allow us to obtain the droplet image in the direction perpendicular to

TABLE I. Characteristics of the rotating ^{3}He$_{1500}$ droplet configurations calculated in this work. O: oblate configurations, P: prolate configurations, and O*: metastable oblate configurations. Λ and Ω are the dimensionless angular momentum and velocity, and $\mathcal{R}$ is the Routhian. AR is the aspect ratio, $AR = a_x/b_y$ (AR = 1 for oblate configurations), and $\mathcal{I}/I_{sph}$ is the DFT moment of inertia in units of that of a sphere of sharp radius, $\mathcal{I}_{sph} = (2/5)m\,r_0^2\,N^{5/3}$ (see the text for the meaning of the other entries).

|	Λ	Ω	a_x (Å)	b_y (Å)	c_z (Å)	AR	b_y^3/V	a_x/c_z	$\mathcal{I}/\mathcal{I}_{sph}$	$\mathcal{R}$ (K)
O	0.1755	0.1000	28.15	28.15	27.88	1	0.242	1.010	1.045	−2538.86
O	0.3759	0.2093	28.47	28.47	27.26	1	0.251	1.044	1.069	−2516.80
O	0.5216	0.2832	28.83	28.83	26.59	1	0.260	1.084	1.096	−2491.30
O	0.7858	0.4015	29.68	29.68	25.01	1	0.284	1.187	1.165	−2426.83
O	1.0553	0.5000	30.76	30.76	23.12	1	0.316	1.330	1.256	−2340.33
O	1.1352	0.5250	31.10	31.10	22.53	1	0.327	1.380	1.287	−2311.30
O	1.2217	0.5500	31.49	31.49	21.89	1	0.339	1.439	1.322	−2278.32
O	1.2527	0.5585	31.63	31.63	21.66	1	0.344	1.460	1.335	−2266.12
O	1.2800	0.5665	31.71	31.71	21.47	1	0.347	1.477	1.345	−2254.65
O*	1.3774	0.5900	32.21	32.21	20.72	1	0.363	1.555	1.389	−2215.34
O*	1.5984	0.6364	33.28	33.28	19.05	1	0.401	1.747	1.495	−2119.10
P	1.2800	0.5665	31.85	31.56	21.47	1.009	0.345	1.483	1.345	−2254.65
P	1.2850	0.5652	33.21	30.27	21.43	1.097	0.301	1.550	1.353	−2252.65
P	1.2900	0.5637	33.89	29.65	21.39	1.143	0.283	1.584	1.362	−2250.65
P	1.3000	0.5605	34.89	28.79	21.30	1.212	0.259	1.638	1.380	−2246.66
P	1.3500	0.5448	37.98	26.37	20.89	1.440	0.199	1.818	1.474	−2227.06
P	1.4000	0.5296	40.17	24.85	20.47	1.616	0.167	1.963	1.573	−2208.02
P	1.4500	0.5168	41.89	23.74	20.07	1.765	0.145	2.088	1.670	−2201.98
P	1.5000	0.5027	43.52	22.73	19.64	1.915	0.128	2.216	1.776	−2171.43
P	1.6000	0.4759	46.40	21.03	18.80	2.206	0.101	2.467	2.001	−2136.74
P	1.7000	0.4503	48.98	19.56	17.94	2.504	0.0813	2.730	2.247	−2103.91
P	1.8000	0.4252	51.37	18.20	17.02	2.823	0.0655	3.018	2.519	−2072.87
P	1.9000	0.3997	53.66	16.84	16.01	3.187	0.0519	3.352	2.829	−2043.62
P	2.0000	0.3716	55.96	15.29	14.75	3.660	0.0389	3.795	3.203	−2016.24
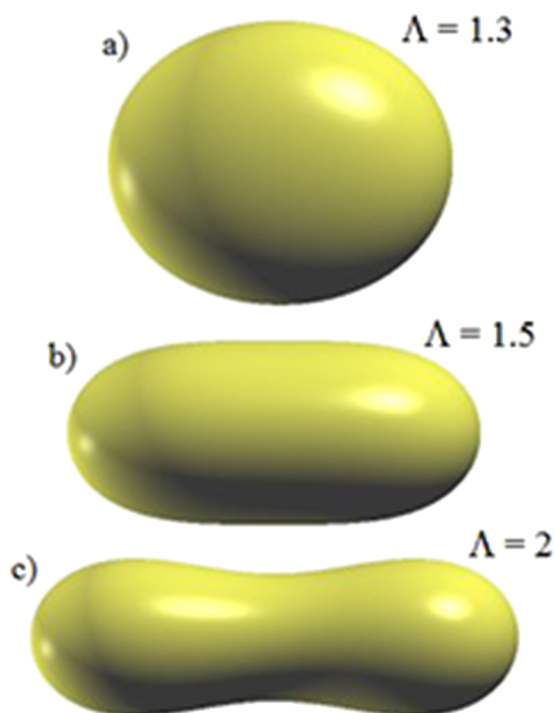
FIG. 2. Some prolate $^3He_{1500}$ equilibrium configurations represented by their sharp density surfaces (not to scale).

the detector plane.[23] Angular momentum is also a key quantity that has eluded *direct* experimental determination. When the diffraction images correspond to droplets that have been unambiguously detected with their rotation axis aligned with the x-ray beam,[10,39] the calculated aspect ratio $AR = a_x/b_y$ as a function of Λ might allow to
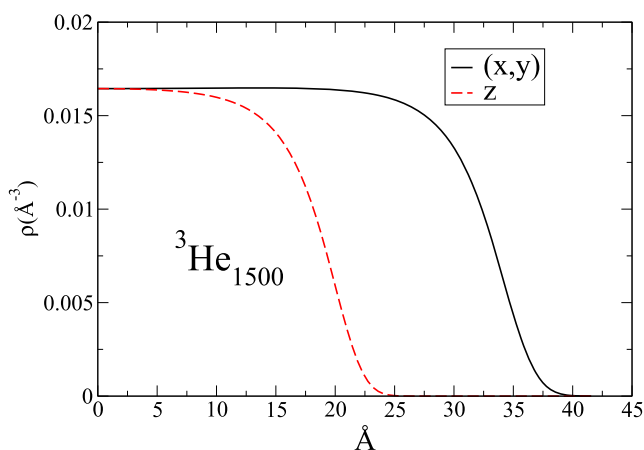

FIG. 3. Density profile of the oblate $\Omega = 0.6364$ configuration along the x and y axes (black solid line) and along the rotation z-axis (red dashed line). The densities have reflective symmetry with respect to the coordinate planes.
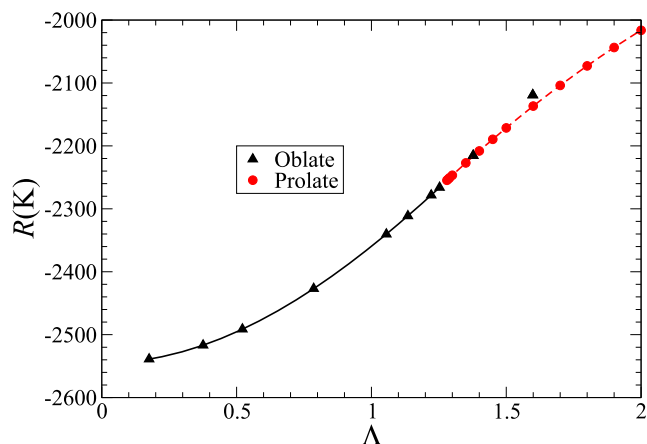
FIG. 4. Routhian $\mathcal{R}[\rho]$ as a function of Λ. Black triangles: oblate configurations. Red circles: prolate configurations. The lines are cubic splines of the calculated points.

determine the angular momentum of the droplet using the classical or DFT-TF calculations. The fact that both approaches sensibly yield the same $\Omega(\Lambda)$ relationship in the oblate branch renders this model-dependent procedure to determine the angular momentum and velocity of oblate ^3He droplets very reliable up to fairly large Λ values.

As mentioned, so far there is no direct experimental information on the angular momentum of the rotating droplets, and the rotational axis has been determined only in a few cases. The shape of ^4He droplets has been determined by parameterizing them and computing the wide-angle diffraction patterns they produce, iteratively
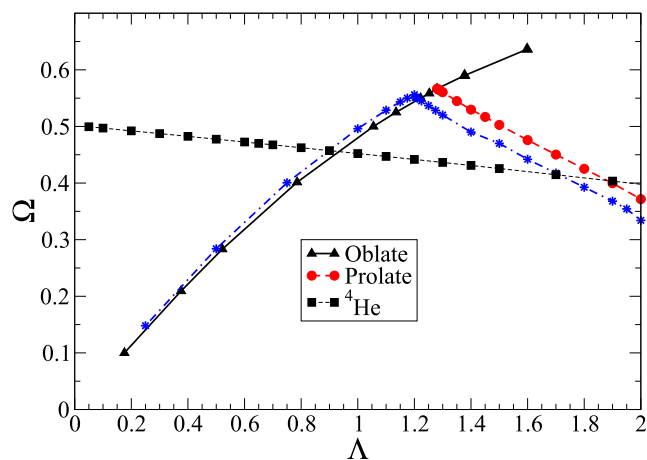

FIG. 5. Rescaled angular velocity Ω vs rescaled angular momentum Λ. Black triangles: oblate configurations. Red circles: prolate configurations. The lines are cubic splines of the displayed points. The stars connected with a blue dotted–dashed line are the classical rotating drop result of Ref. 15. For the sake of comparison, the $\Omega(\Lambda)$ curve corresponding to vortex-free ^4He droplets is also shown (black squares).

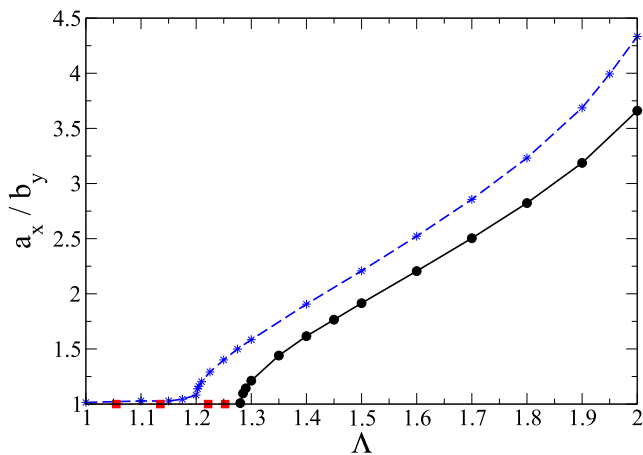**FIG. 6**. Aspect ratio $AR = a_x/b_y$ vs Λ curve for ^{3}He droplets. $AR = 1$ corresponds to oblate configurations. The starred symbols connected by a dashed blue line are the classical model results.[16]

FIG. 8. b_y^3/V ratio vs a_x/c_z curve for ^{3}He. Black triangles: oblate configurations. Open triangles: metastable oblate configurations. Red circles: prolate configurations. The starred symbols connected by a blue dashed line are the classical model results.[16]

changing the parameters until matching the experimental diffraction patterns.[11] This procedure does not provide the angular momentum or the direction of the rotation axis but supplies interesting information, in particular, the distance of the COM to the droplet surface along the axes used to describe the parameterized droplet surface. This is the rationale for displaying b_y^3/V vs the ratio a_x/c_z in Fig. 8, which can be used to compare the classical and DFT results. The dashed line shows the classical model result of Ref. 16. The agreement between classical and DFT-TF calculations for ^{3}He droplets is good and even remarkable for prolate configurations. A similar good agreement was found between parameterized, vortex-hosting DFT and classical ^{4}He droplets.[11,17]
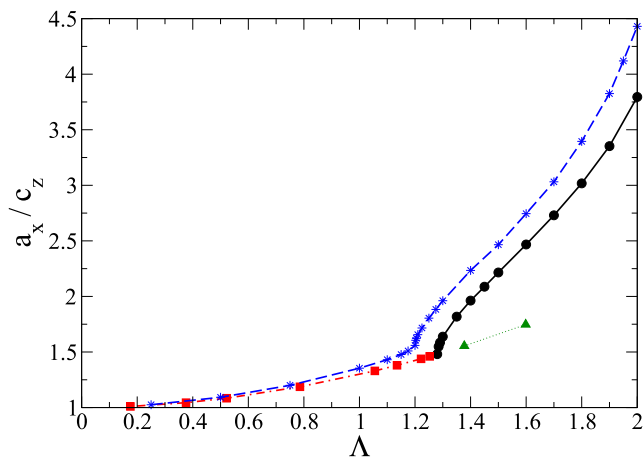
IV. SUMMARY AND OUTLOOK

We have studied the rotating ^{3}He droplets by combining a semiclassical Thomas–Fermi approach with the well-established DFT formalism for liquid helium. We have shown that classical models for the equilibrium shapes of rotating drops that are subject to surface tension and centrifugal forces alone work remarkably well when they are applied to a nanoscopic quantum object as ^{3}He droplets. Minor differences appear between their results and the DFT ones, which are likely due to a better description of the droplet surface and to quantum kinetic energy contributions in the microscopic approach that, together with curvature energy and compressibility effects, are lacking in classical models. Conceptually, the classical model of droplets subjected to surface tension[13] is closer to the liquid drop model (LDM),[41] whereas the DFT approach is closer to the finite-range droplet model,[42] a sophisticated extension of the LDM.

The DFT approach to rotating helium nanodroplets has previously been applied to isotopically pure ^{4}He superfluid droplets, allowing us to clarify the influence of vortex arrays on their equilibrium shapes[40] and disclosing the presence of capillary waves and their interplay with vortices.[17,43] We have shown here that the DFT approach allows us to describe as well the rotating quantum normal fluid ^{3}He droplets on a microscopic and firm basis. The availability of an accurate theoretical framework for studying spinning droplets of both isotopes is a crucial ingredient necessary for addressing a far more challenging system, namely, rotating mixed ^{3}He–^{4}He droplets at very low temperatures, a work that is now in progress.

FIG. 7. a_x/c_z ratio vs Λ curve for ^{3}He. Red squares correspond to oblate configurations, and black dots correspond to prolate configurations. Green triangles correspond to metastable oblate configurations. The starred symbols connected by a dashed blue line are the classical model results.[16]
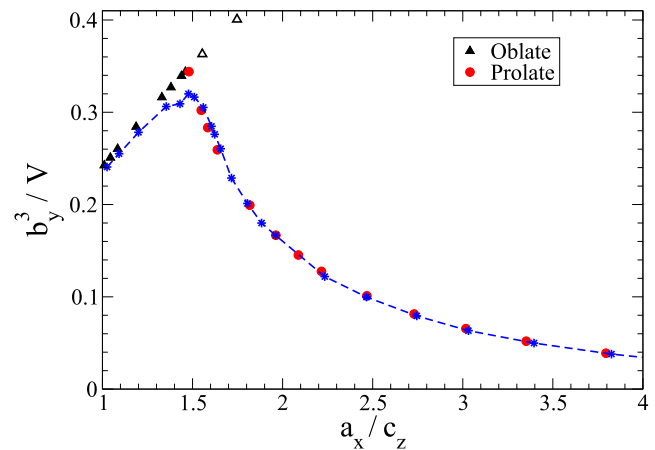
APPENDIX: ROTATING TF MODEL

We introduce in this appendix the basics of the rotating TF model, as discussed in Ref. 25. In a rotating ^{3}He droplet, the local momentum distribution of its atoms is altered due to the motion of the droplet as a whole. The Fermi sphere is displaced from $\mathbf{k} = 0$,

$$|\mathbf{k}(\mathbf{r}) - \mathbf{K}_R(\mathbf{r})| \leq k_F(\mathbf{r}), \tag{A1}$$

where $\hbar k_F(\mathbf{r})$ is the Fermi momentum at point $\mathbf{r}$ and $\hbar \mathbf{K}_R(\mathbf{r})$ is the local momentum due to rotation, namely,

$$\mathbf{K}_R(\mathbf{r}) = \frac{m}{\hbar} \boldsymbol{\omega} \times \mathbf{r}. \tag{A2}$$

It is straightforward to obtain the expressions for quantities such as the particle number N,

$$N = \frac{2}{(2\pi)^3} \int d\mathbf{r} \int_{|\mathbf{k}(\mathbf{r}) - \mathbf{K}_R(\mathbf{r})| \leq k_F(\mathbf{r})} d\mathbf{k} = \frac{1}{3\pi^2} \int d\mathbf{r}\, k_F^3(\mathbf{r}). \tag{A3}$$

Thus, the particle density is

$$\rho(\mathbf{r}) = \frac{k_F^3(\mathbf{r})}{3\pi^2} \Rightarrow k_F(\mathbf{r}) = [3\pi^2 \rho(\mathbf{r})]^{1/3}. \tag{A4}$$

The kinetic energy is similarly obtained by

$$T = \frac{2}{(2\pi)^3} \int d\mathbf{r} \int_{|\mathbf{k}(\mathbf{r}) - \mathbf{K}_R(\mathbf{r})| \leq k_F(\mathbf{r})} d\mathbf{k}\, \frac{\hbar^2 k^2}{2m}. \tag{A5}$$

As done in Eq. (A3) for N, if $\mathbf{k}(\mathbf{r}) - \mathbf{K}_R(\mathbf{r}) \equiv \mathbf{k}'(\mathbf{r})$, the Jacobian is $|J| = 1$ and the kinetic energy becomes

$$T = \frac{\hbar^2}{2m} \int d\mathbf{r} \frac{2}{(2\pi)^3} \int_{|\mathbf{k}'(\mathbf{r})| \leq k_F(\mathbf{r})} d\mathbf{k}' [k'^2 + K_R^2] \tag{A6}$$

[the integral of the cross term $2\,\mathbf{k}'(\mathbf{r}) \cdot \mathbf{K}_R(\mathbf{r})$ is zero]. Hence,

$$T = \frac{\hbar^2}{2m} \int d\mathbf{r} \frac{2}{(2\pi)^3} \left[\frac{4\pi}{5} k_F^5(\mathbf{r}) + K_R^2(\mathbf{r}) \frac{4\pi}{3} k_F^3(\mathbf{r}) \right] \tag{A7}$$

and

$$T = \frac{\hbar^2}{2m} \int d\mathbf{r} \frac{3}{5} (3\pi^2)^{2/3} \rho^{5/3}(\mathbf{r}) + \frac{\hbar^2}{2m} \int d\mathbf{r}\, K_R^2(\mathbf{r})\, \rho(\mathbf{r}). \tag{A8}$$

The first term is the ordinary TF kinetic energy. The second term is easily identified with the rotation energy. If we take $\boldsymbol{\omega}$ in the z direction [$\boldsymbol{\omega} = \omega(0,0,1)$] and substitute $\mathbf{K}_R(\mathbf{r})$ by its expression Eq. (A2), one gets

$$\frac{\hbar^2}{2m} \int d\mathbf{r}\, K_R^2(\mathbf{r})\, \rho(\mathbf{r}) = \frac{1}{2} m\omega^2 \int d\mathbf{r}(x^2 + y^2)\rho(\mathbf{r}) \equiv \frac{1}{2} \mathcal{I}\omega^2, \tag{A9}$$

where we have introduced the definition of the moment of inertia $\mathcal{I}$ about the z-axis. It is worth seeing that the TF approximation leads naturally to a rigid body rotation in the case of fermions.

Let us calculate the angular momentum,

$$
\begin{aligned}
\mathbf{L} &= \frac{2}{(2\pi)^3} \hbar \int d\mathbf{r} \int_{|\mathbf{k}(\mathbf{r}) - \mathbf{K}_R(\mathbf{r})| \leq k_F(\mathbf{r})} d\mathbf{k}\, (\mathbf{r} \times \mathbf{k}) \\
&= \frac{2}{(2\pi)^3} \hbar \int d\mathbf{r} \int_{|\mathbf{k}'(\mathbf{r})| \leq k_F(\mathbf{r})} d\mathbf{k}'\, \mathbf{r} \times [\mathbf{k}' + \mathbf{K}_R(\mathbf{r})] \\
&= \hbar \int d\mathbf{r} [\mathbf{r} \times \mathbf{K}_R(\mathbf{r})]\rho(\mathbf{r}) = m \int d\mathbf{r} [\mathbf{r} \times (\boldsymbol{\omega} \times \mathbf{r})]\rho(\mathbf{r}).
\end{aligned}
\tag{A10}
$$

In Cartesian coordinates,

$$\mathbf{r} \times (\boldsymbol{\omega} \times \mathbf{r}) = \omega[-xz\hat{i} - yz\hat{j} + (x^2 + y^2)\hat{k}]. \tag{A11}$$

Thus, if $\rho(x, y, z)$ is such that

$$\rho(x,y,z) = \rho(-x,y,z) \quad \text{and} \quad \rho(x,y,z) = \rho(x,-y,z) \tag{A12}$$

or

$$\rho(x,y,z) = \rho(x,y,-z), \tag{A13}$$

we get

$$\mathbf{L} = m\boldsymbol{\omega} \int d\mathbf{r}(x^2 + y^2)\rho(\mathbf{r}) = \mathcal{I}\boldsymbol{\omega}. \tag{A14}$$

In their classical paper on rotating drops under surface tension, Brown and Scriven[13] assumed that droplets have reflective symmetry about their equator plane ($z = 0$) and at least one meridional plane of reflective symmetry (either $x = 0$ or $y = 0$). We have assumed that $z = 0$ is a reflective plane of symmetry and have taken Eq. (A14) for the definition of $\mathbf{L}$.

REFERENCES

[1] C. Ebner and D. O. Edwards, Phys. Rep. **2C**, 77 (1970).

[2] J. P. Toennies, Annu. Rev. Phys. Chem. **55**, 1 (2004).

[3] J. P. Toennies and A. F. Vilesov, Angew. Chem. Phys. **43**, 2622 (2004).

[4] K. K. Lehmann and G. Scoles, Science **279**, 2065 (1998).

[5] S. Grebenev, J. P. Toennies, and A. F. Vilesov, Science **279**, 2083 (1998).

[6] B. G. Sartakov, J. P. Toennies, and A. F. Vilesov, J. Chem. Phys. **136**, 134316 (2012).

[7] M. Barranco, R. Guardiola, S. Hernández, R. Mayol, J. Navarro, and M. Pi, J. Low Temp. Phys. **142**, 1 (2006).

[8] F. Ancilotto, M. Barranco, F. Coppens, J. Eloranta, N. Halberstadt, A. Hernando, D. Mateo, and M. Pi, Int. Rev. Phys. Chem. **36**, 621 (2017).

[9] R. M. Tanyag, C. F. Jones, C. Bernando, S. M. O'Connell, D. Verma, and A. F. Vilesov, in *Theoretical and Computational Chemistry Series*, edited by O. Dulieu and A. Osterwalder (Royal Society of Chemistry, Cambridge, 2018), No. 11, p. 389.

[10] L. F. Gomez, K. R. Ferguson, J. P. Cryan, C. Bacellar, R. M. P. Tanyag, C. Jones, S. Schorb, D. Anielski, A. Belkacem, C. Bernando, R. Boll, J. Bozek, S. Carron, G. Chen, T. Delmas, L. Englert, S. W. Epp, B. Erk, L. Foucar, R. Hartmann, A. Hexemer, M. Huth, J. Kwok, S. R. Leone, J. H. S. Ma, F. R. N. C. Maia, E. Malmerberg, S. Marchesini, D. M. Neumark, B. Poon, J. Prell, D. Rolles, B. Rudek, A. Rudenko, M. Seifrid, K. R. Siefermann, F. P. Sturm, M. Swiggers, J. Ullrich, F. Weise, P. Zwart, C. Bostedt, O. Gessner, and A. F. Vilesov, Science **345**, 906 (2014).

[11] B. Langbehn, K. Sander, Y. Ovcharenko, C. Peltz, A. Clark, M. Coreno, R. Cucini, M. Drabbels, P. Finetti, M. Di Fraia, L. Giannessi, C. Grazioli, D. Iablonskyi, A. C. LaForge, T. Nishiyama, V. Oliver Álvarez de Lara, P. Piseri, O. Plekan, K. Ueda, J. Zimmermann, K. C. Prince, F. Stienkemeier, C. Callegari, T. Fennel, D. Rupp, and T. Möller, Phys. Rev. Lett. **121**, 255301 (2018).

[12]O. Gessner and A. F. Vilesov, Annu. Rev. Phys. Chem. **70**, 173 (2019).

[13]R. A. Brown and L. E. Scriven, Proc. R. Soc. London, Ser. A **371**, 331 (1980).

[14]C.-J. Heine, IMA J. Numer. Anal. **26**, 723 (2006).

[15]S. L. Butler, M. R. Stauffer, G. Sinha, A. Lilly, and R. J. Spiteri, J. Fluid Mech. **667**, 358 (2011).

[16]K. A. Baldwin, S. L. Butler, and R. J. A. Hill, Sci. Rep. **5**, 7660 (2015).

[17]F. Ancilotto, M. Pi, and M. Barranco, Phys. Rev. B **97**, 184515 (2018).

[18]S. Stringari and J. Treiner, J. Chem. Phys. **87**, 5021 (1987).

[19]D. Mateo, M. Pi, J. Navarro, and J. P. Toennies, J. Chem. Phys. **138**, 044321 (2013).

[20]F. Garcias, Ll. Serra, M. Casas, and M. Barranco, J. Chem. Phys. **108**, 9102 (1998).

[21]R. Guardiola and J. Navarro, Phys. Rev. A **71**, 035201 (2005).

[22]M. P. de Lara-Castells, P. Villarreal, G. Delgado-Barrio, and A. O. Mitrushchenkov, J. Chem. Phys. **131**, 194101 (2009).

[23]D. Verma, S. M. O. O'Connell, A. J. Feinberg, S. Erukala, R. M. Tanyag, C. Bernando, W. Pang, C. A. Saladrigas, B. W. Toulson, M. Borgwardt, N. Shivaram, M.-F. Lin, A. Al Haddad, W. Jäger, C. Bostedt, P. Walter, O. Gessner, and A. F. Vilesov, arXiv:2003.07466 (2020).

[24]A. Leal, D. Mateo, M. Pi, M. Barranco, and J. Navarro, J. Chem. Phys. **139**, 174308 (2013).

[25]B. Grammaticos, Phys. Rev. C **17**, 1244 (1978).

[26]L. Munchow and H. Schulz, J. Phys. G: Nucl. Phys. **5**, 527 (1979).

[27]B. Grammaticos and T. Sami, J. Phys. G: Nucl. Phys. **7**, 1063 (1981).

[28]M. Barranco, M. Pi, S. M. Gatica, E. S. Hernández, and J. Navarro, Phys. Rev. B **56**, 8997 (1997).

[29]R. J. Lombard, Ann. Phys. **77**, 380 (1973).

[30]A. deShalit and H. Feshbach, *Theoretical Nuclear Physics: Vol. I: Nuclear Structure* (John Wiley & Sons, New York, 1974).

[31]A. Bohr and B. R. Mottelson, *Nuclear Structure* (W. A. Benjamin, Reading, MA, 1975), Vol. II.

[32]P. Ring and P. Schuck, *The Nuclear Many-Body Problem* (Springer-Verlag, New York, 1980).

[33]M. Pi, F. Ancilotto, F. Coppens, N. Halberstadt, A. Hernando, A. Leal, D. Mateo, R. Mayol, and M. Barranco, ^{4}He-DFT BCN-TLS: A Computer Package for Simulating Structural Properties and Dynamics of Doped Liquid Helium-4 Systems, https://github.com/bcntls2016/DFT-Guide/blob/master/dft-guide.pdf.

[34]M. Barranco, F. Coppens, N. Halberstadt, A. Hernando, A. Leal, D. Mateo, R. Mayol, and M. Pi, Zero temperature DFT and TDDFT for ^{4}He: A short guide for practitioners, https://github.com/bcntls2016/.

[35]K. Penanen, M. Fukuto, R. K. Heilmann, I. F. Silvera, and P. S. Pershan, Phys. Rev. **62**, 9621 (2000).

[36]H. Lamb, *Hydrodynamics*, 6th ed. (Dover, New York, 1945).

[37]F. Coppens, F. Ancilotto, M. Barranco, N. Halberstadt, and M. Pi, Phys. Chem. Chem. Phys. **19**, 24805 (2017).

[38]We have analyzed the density profiles along the coordinate axes for some oblate and prolate configurations, and have found that surface diffuseness hardly depends on the deformation of the droplet.

[39]C. Bernando, R. M. P. Tanyag, C. Jones, C. Bacellar, M. Bucher, K. R. Ferguson, D. Rupp, M. P. Ziemkiewicz, L. F. Gomez, A. S. Chatterley, T. Gorkhover, M. Müller, J. Bozek, S. Carron, J. Kwok, S. L. Butler, T. Möller, C. Bostedt, O. Gessner, and A. F. Vilesov, Phys. Rev. B **95**, 064510 (2017).

[40]F. Ancilotto, M. Pi, and M. Barranco, Phys. Rev. B **91**, 100503(R) (2015).

[41]S. Cohen, F. Plasil, and W. J. Swiatecki, Ann. Phys. **82**, 557 (1974).

[42]P. Möller, R. J. Nix, W. D. Myers, and W. J. Swiatecki, At. Data Nucl. Data Tables **59**, 185 (1995).

[43]S. M. O. O'Connell, R. M. P. Tanyag, D. Verma, Ch. Bernando, W. Pang, C. Bacellar, C. A. Saladrigas, J. Mahl, B. W. Toulson, Y. Kumagai, P. Walter, F. Ancilotto, M. Barranco, M. Pi, Ch. Bostedt, O. Gessner, and A. F. Vilesov, "Angular Momentum in Rotating Superfluid Droplets," Phys. Rev. Lett. (to be published) (2020); arXiv:1910.12926.